THE JOURNAL OF BIOLOGICAL CHEMISTRY VOL. 287, NO. 40, pp. 33883–33896, September 28, 2012
Published in the U.S.A.

Znt7-null Mice Are More Susceptible to Diet-induced Glucose Intolerance and Insulin Resistance*[S]

Received for publication, March 5, 2012, and in revised form, July 11, 2012 Published, JBC Papers in Press, August 1, 2012, DOI 10.1074/jbc.M111.309666

Liping Huang[‡§1], Catherine P. Kirschke[‡], Yu-An E. Lay[§2], Lauren B. Levy[§3], Danielle E. Lamirande[‡], and Patrick H. Zhang[‡]

From the [‡]United States Department of Agriculture/Agricultural Research Service/Western Human Nutrition Research Center, Obesity and Metabolism Research Unit, Davis, California 95616 and the [§]Department of Nutrition, University of California, Davis, California 95616

Background: Zinc transporter 7 (ZnT7) influences insulin synthesis/secretion in β-cells.
Results: *Znt7*-null mice have impaired glucose tolerance and are insulin-resistant.
Conclusion: A combination of decreased insulin secretion and increased insulin resistance accounts for the glucose intolerance in *Znt7*-null mice.
Significance: The study provides direct evidence that zinc homeostasis is crucial for glucose/insulin metabolism.

The *Znt7* gene encodes a ubiquitously expressed zinc transporter that is involved in transporting cytoplasmic zinc into the Golgi apparatus and a ZnT7-containing vesicular compartment. Overexpression of ZnT7 in the pancreatic β-cell stimulates insulin synthesis and secretion through regulation of insulin gene transcription. In this study, we demonstrate that ZnT7 is expressed in the mouse skeletal muscle. The activity of the insulin signaling pathway was down-regulated in myocytes isolated from the femoral muscle of *Znt7* knock-out (KO) mice. High fat diet consumption (45% kcal) induced weight gain in male *Znt7* KO mice but not female *Znt7* KO mice. Male *Znt7* KO mice fed the high fat diet at 5 weeks of age for 10 weeks exhibited hyperglycemia in the non-fasting state. Oral glucose tolerance tests revealed that male *Znt7* KO mice fed the high fat diet had severe glucose intolerance. Insulin tolerance tests showed that male *Znt7* KO mice were insulin-resistant. Diet-induced insulin resistance in male *Znt7* KO mice was paralleled by a reduction in mRNA expression of *Insr*, *Irs2*, and *Akt1* in the primary skeletal myotubes isolated from the KO mice. Overexpression of ZnT7 in a rat skeletal muscle cell line (L6) increased *Irs2* mRNA expression, Irs2 and Akt phosphorylation, and glucose uptake. We conclude that a combination of decreased insulin secretion and increased insulin resistance accounts for the glucose intolerance observed in *Znt7* KO mice.

Cellular zinc (Zn^{2+}) homeostasis is tightly controlled through regulation of zinc transporters for either zinc efflux/sequestration (ZnT/Slc30 family) or zinc influx (ZIP/Slc39 family). Members in the same family of zinc transporters have similar protein structures. For example, ZnT proteins (ZnT1 to -10) have six transmembrane (TM)[4] domains and a histidine-rich loop between TM domains IV and V (1), except for ZnT5, which has an extra 10 TM domains at the N-terminal end of the protein (2, 3). ZIP proteins (ZIP1 to -14) contain eight TM domains and a histidine-rich loop between TM domains III and IV (4). Except for the ZnT5 isoform b, which can mediate bidirectional zinc transport (5), ZnT proteins function to transport zinc out of the cell or into subcellular compartments when cytoplasmic zinc is replete. On the other hand, ZIP proteins act to transport zinc into the cell or out to the cytoplasm from intracellular storage compartments when cytoplasmic zinc is depleted (6).

Connections between zinc homeostasis and body adiposity and diabetes remain largely unknown. Recently, it has been shown that ZnT8, a ZnT protein predominantly expressed in β-cells of the pancreas, is associated with human type 1 and type 2 diabetes (7, 8). In pancreatic β-cells, ZnT8 is abundantly expressed in the insulin-containing secretory granules near the plasma membrane (9). It plays a role in translocation of cytoplasmic zinc into the insulin-containing granules for insulin crystallization (10). A single-nucleotide polymorphism (SNP) at amino acid position 325 in ZnT8 is associated with diabetes (11). The ZnT8 with Arg-325 has strong autoimmunity that can lead to development of type 1 diabetes in children (12, 13). Arg-325 polymorphism of ZnT8 is also associated with susceptibility to type 2 diabetes in humans (14–16). Mice lacking ZnT8 have low circulating insulin concentrations due to a defect in insulin secretion from pancreatic β-cells (17–19). Interestingly, no obvious impairment of glucose metabolism is seen in *Znt8* KO mice (17, 19).

ZnT7 is a zinc transporter involved in the translocation of cytoplasmic zinc into the Golgi apparatus and ZnT7-containing vesicles in the cell (20). Overexpression of ZnT7 in insulin-

* This work was supported by United States Department of Agriculture, Agricultural Research Service, Projects 5306-515-30-014–00D and 5306-515-20-007-00D.
[S] This article contains supplemental Table 1 and Fig. 1.
[1] To whom correspondence should be addressed: USDA/ARS/Western Human Nutrition Research Center, 430 West Health Sciences Dr., University of California, Davis, CA 95616. Tel.: 530-754-5756; Fax: 530-752-5295; E-mail: liping.huang@ars.usda.gov.
[2] Present address: UCD Internal Medicine, Musculoskeletal Diseases of Aging Research and Education Group Research II, 4625 2nd Ave., Suite 1002, Sacramento, CA 95817.
[3] Present address: Satellite Healthcare, 801 Davis St., San Leandro, CA 94577.

[4] The abbreviations used are: TM, transmembrane; HF, high fat; LF, low fat; MEM, minimum essential medium; 2-DG, 2-deoxyglucose; pAkt, phosphorylated Akt; AUC, area under the curve.

secreting β-cells results in elevated insulin synthesis and secretion (21). *Znt7* KO mice display low body zinc status (22). As a result, *Znt7* KO mice show a phenotype of poor growth, a classic manifestation of zinc deficiency (23). However, *Znt7* KO mice do not show any sign of hair growth abnormality and dermatitis, signs that are commonly seen in dietary zinc-deficient animals and humans (23). Dietary zinc supplementation cannot alleviate the symptoms of zinc deficiency in *Znt7* KO mice (22). Another notable feature of *Znt7* KO mice is that they exhibit decreased adiposity with low circulating leptin level (22). Leptin is a hormone secreted from adipocytes that regulates food intake, energy expenditure, and neuroendocrine function (24, 25). Low levels of circulating leptin observed in *Znt7* KO mice are consistent with previous studies that zinc deficiency decreases blood leptin level, whereas zinc supplementation increases this level (26). *Znt7* KO mice also display slightly higher blood glucose levels than the control 2 h after an oral glucose administration (22), suggesting that glucose homeostasis may be affected by the *Znt7*-null mutation.

Recently, using a rat pancreatic β-cell line overexpressing ZnT7, we demonstrated that ZnT7 influenced insulin synthesis and secretion (21). However, it is currently unclear whether ZnT7 affects body glucose homeostasis in mice by regulating the insulin signaling pathway in insulin-sensitive peripheral tissues. In light of the potential role of ZnT7 in glucose homeostasis and pathogenesis of diabetes, we sought to examine and compare the physiological consequences of diet-induced obesity between *Znt7* KO and control mice. *Znt7* KO and control mice were fed either a high fat diet (45% kcal) or a low fat diet (10% kcal) at 5 weeks of age for 10–12 weeks. Body weight gain, fat accumulation, oral glucose tolerance, insulin tolerance, and blood insulin levels were examined in these mice. In addition, mRNA expression of insulin signaling pathway-associated genes in the skeletal muscle, a tissue responsible for 70–90% of glucose disposal following a carbohydrate load (27), was studied. Our results showed that male *Znt7* KO mice were more susceptible to diet-induced glucose intolerance and insulin resistance than the control. Fasting blood insulin levels in male *Znt7* KO mice fed the high fat diet was lower than the control. Our data also demonstrated that ZnT7 affected *Irs2* (insulin receptor substrate 2) expression and phosphorylation of Irs2 and Akt (v-*akt* murine thymoma viral oncogene homolog) in *Znt7* KO myotubes as well as L6 myotubes overexpressing ZnT7.

EXPERIMENTAL PROCEDURES

Animals and Diets—The congenic *Znt7* KO and control (C57BL/6) mice (22) were housed in a temperature-controlled room at 22–24 °C with a 12-h light/dark cycle and fed a standard laboratory chow diet (Laboratory Rodent Diet 5001, LabDiet, Brentwood, MO) and double-distilled water *ad libitum*. Where indicated, mice at 5 weeks of age were fed either a high or a low fat diet in the study. Diets containing a defined amount of fat (10% kcal, low fat, D12450B, or 45% kcal, high fat, D12451) were purchased from Research Diets (New Brunswick, NJ). Body weights were recorded biweekly from 5 to 12 weeks of age. Animal experiments were conducted in accordance with National Institutes of Health guidelines for the care and use of experimental animals and were approved by the Institutional Animal Care and Use Committee of the University of California (Davis, CA).

Analyses—After 12 weeks of feeding, mice were fasted for 16–18 h and weighed. Mice were anesthetized by intraperitoneal injection of 250 mg/kg trimbromoethanol (Avertin®, Aldrich). Blood was collected from retro-orbital bleeding followed by cardiac puncture. Blood glucose levels were determined using a OneTouch UltraMini meter (LifeScan, Milpitas, CA). Serum was isolated for insulin, triglyceride, and cholesterol assays. Insulin was measured using a mouse insulin ELISA kit (ALPCO, Salem, NH). Total cholesterol and triglycerides were determined using cholesterol-E and L-type TGH assays, respectively, from Wako (Richmond, VA).

Fat Pad Isolation and Body Composition—After 12 weeks of feeding, mice were fasted for 16–18 h, weighed, and euthanized by cardiac puncture while anesthetized. Epididymal, periovarian, retroperitoneal, femoral, and mesenteric fat pads were isolated, weighed, snap-frozen, and stored at −80 °C. The remaining carcasses were weighed and stored at −20 °C in sealed containers until analysis. The chemical body composition analysis of the remaining carcasses was done as described previously (28).

Antibodies—The affinity-purified ZnT7 polyclonal antibody was made as described previously (20). The peptide-blocked ZnT7 antibody was obtained by incubation of the ZnT7 antibody with a peptide that was used to raise the ZnT7 antibody (20) at a ratio of 5:1 (peptide/antibody) in 1× PBS, pH 7.4, containing 2% mouse serum for 2 h at room temperature. The Alexa 488-conjugated and HRP-conjugated goat anti-rabbit antibodies were purchased from Invitrogen and Pierce, respectively.

Immunohistochemistry—Mouse femoral muscles were isolated from male C57Bl/6 and *Znt7* KO mice. Tissues were rinsed once in 1× PBS, pH 7.4, and immersed in 4% paraformaldehyde in 1× PBS. Tissues were then dehydrated in 80, 95, and 100% FLEX (Richard-Allan Scientific), cleared in ClearRite 3 (Richard-Allan Scientific), infiltrated, and embedded in paraffin (Richard-Allan Scientific) (29). Tissue was sectioned in 5-μm thickness. Mounted tissue sections were deparaffinized in xylene and rehydrated (29). Antigen retrieval was done by boiling the slides in 100 μM Tris-HCl buffer, pH 10, for 20 min followed by 20 min of cooling at room temperature. Blocking was accomplished by applying 5% goat serum diluted in 1× PBS (pH 7.4) at room temperature for 1 h. Tissue was then incubated with the ZnT7 antibody (1:750 diluted in 1× PBS containing 2% mouse serum). Slides were washed with 1× PBS and stained using a Vectastain ABC kit and a DAB substrate (Vector Laboratories, Burlingame, CA). Tissue sections were covered with coverslips using Permount mounting medium (Fisher). Photomicrographs were obtained by a Nikon Eclipse 800 microscope equipped with a digital camera.

Isolation and Culture of Primary Myoblasts and Myotubes—The hind limbs of *Znt7* KO and control neonatal mice (3–4 days old) were removed, and skeletal muscles were dissected from the bones. Muscles were minced with fine scissors into small fragments. The minced muscle was subjected to proteolytic enzyme treatment in 0.5–1 ml of 1× PBS containing

dispase (2.4 units/ml, grade II; Sigma), collagenase (1%, class D; Roche Applied Science), and 2.5 mM $CaCl_2$ at 37 °C for 30 min with occasional mixing. The slurry was then centrifuged at 350 × *g* at room temperature for 5 min. The pellet was resuspended in a selective medium consisting of 80% Ham's F-10 (Invitrogen), 20% fetal bovine serum (FBS; Invitrogen), 2.5 ng/ml basic fibroblast growth factor (Gemini Bio-Products, West Sacramento, CA), 200 units/ml penicillin G, and 200 μg/ml streptomycin (Invitrogen). The cell suspension was passed through a 70-μm cell strainer (BD Biosciences) and plated in collagen-coated (Type I, 150 μg/ml; Invitrogen) 100-mm culture dishes in the selective medium. The culture medium was changed after 24 h of incubation. Myoblasts in the mixture of myoblasts and fibroblasts were enriched by 4–5 rounds of a selection procedure as described (30). The purity of myoblasts was determined by positive staining of desmin (supplemental Fig. 1), a protein only expressed in myogenic cells (31). After a pure population of myoblasts was obtained, cells were maintained in a growth medium consisting of 40% Ham's F-10, 40% DMEM, 20% FBS, 2.5 ng/ml basic fibroblast growth factor, 100 units/ml penicillin G, and 100 μg/ml streptomycin. Differentiation of primary myoblasts to myotubes was induced by replacing the growth medium with a differentiation medium (DMEM containing 2% horse serum; Invitrogen). Medium was changed daily for 6 days.

Generation, Maintenance, and Differentiation of Stable L6 Cell Lines—L6 cells (myoblasts from rat skeletal muscles) (ATCC, Manassas, VA) with or without expression of the ZnT7-Myc fusion protein were generated by transfecting pcDNA3.1/ZnT7-Myc (20) or pcDNA3.1/Myc vector (Invitrogen) using Lipofectamine™ PLUS™ reagent (Invitrogen). Stably transfected cells were selected and expanded by culturing cells in α-MEM (supplemented with 10% FBS; Invitrogen) containing 400 μg/ml G418. Individual clones were tested for the presence of ZnT7-Myc by RT-PCR and immunocytochemistry (Fig. 4*A*). Three individual L6/ZnT7-Myc cell lines were used in the subsequent RT-PCR and Western blot analyses. Three individual L6/vector lines were also selected as the controls. The G418-resistant cell lines were maintained in α-MEM with 10% FBS without G418. L6/ZnT7-Myc and L6/vector myoblasts were differentiated into myotubes in DMEM supplemented with 2% horse or bovine serum (Invitrogen) for 6–7 days. Medium was changed daily during differentiation.

[^{14}C]2-Deoxyglucose Uptake Assay—L6/ZnT7-Myc (from two individual cell lines) and control cells (from two individual cell lines) were seeded in triplicate in 48-well plates. Cells were allowed to differentiate into myotubes 24 h after seeding for 6–8 days. Sixteen h prior to the uptake assay, medium was replaced with α-MEM containing 0.2% FBS. Cells were then preincubated with serum-free α-MEM containing 75 μM $ZnSO_4$ at 37 °C for 4 h followed by a 60-min incubation in KRH buffer (50 mM HEPES, pH 7.4, 137 mM NaCl, 4.7 mM KCl, 1.85 mM $CaCl_2$, 1.3 mM $MgSO_4$, 0.4% (w/v) fatty acid-free BSA (Fitzgerald)) plus 75 μM $ZnSO_4$ at 37 °C. Next, insulin was added at 0, 10, or 100 nM for 15 min followed by 10 μM [^{14}C]2-DG (45–60 mCi/mmol, 0.1 mCi/ml; PerkinElmer Life Sciences) plus 100 μM cold D-glucose for 15 min. The reaction was stopped by aspirating the uptake medium. Cells were washed four times in ice-cold PBS containing 20 mM glucose and lysed in 400 μl of 50 mM NaOH. Radioactivity was determined by liquid scintillation counting. Protein concentrations were determined using a BCA protein assay kit (Pierce).

Immunofluorescence Microscopy—Primary, L6/ZnT7-Myc, and L6/vec myoblasts were cultured in slide chambers for 48 h. Cells were washed, fixed with 4% paraformaldehyde, and permeabilized with 0.4% saponin (Sigma). Primary antibodies, such as anti-ZnT7 (1:400) and anti-Myc (1:400; Santa Cruz Biotechnology, Inc. (Santa Cruz, CA)), were applied, followed by Alexa 488-conjugated goat anti-rabbit (1:250; Invitrogen) and anti-mouse antibodies (1:250; Invitrogen), respectively. Photomicrographs were obtained by a Nikon Eclipse 800 microscope equipped with a digital camera.

Western Blot Analysis—Myoblasts of both genotypes were seeded in 6-well culture plates at ~50% confluence and grown at 37 °C for 48 h. Cells were washed and incubated with supplement-free DMEM/F-10 medium (1:1 ratio) at 37 °C for 3 h. Cells were then insulin-treated (0 or 100 nM, human insulin; Sigma) at 37 °C for 7 min. For L6/ZnT7-Myc and control myotubes, cells were preincubated with supplement-free DMEM for 3 h and then treated with insulin at 0, 10, or 100 nM for 7 min. After insulin treatment, cells were washed and lysed in 150 μl of ice-cold lysis buffer (50 mM Tris-HCl, pH 8.0, 10 mM NaCl, 1% Nonidet P-40, 5 mM EDTA, 2 mM NaF, 2 mM $Na_4P_2O_7$, and 2 mM Na_3VO_4). Protease inhibitors (Roche Applied Science) were added just before use. Lysate was sonicated for 5 s in 0.5 s on/1.0 s off cycles at 11% on ice using a Branson digital sonifier. Protein concentrations were determined using a BCA protein assay kit (Pierce). Eleven (primary myoblasts) or 15 (L6/ZnT7-Myc and control myotubes) micrograms of protein lysate were loaded on 7.5% (primary myoblasts) or 4–20% (L6/ZnT7-Myc and control myotubes) Tris/glycine gels (Bio-Rad). Separated proteins were electroblotted onto Immobilon-P membranes (Millipore, Billerica, MA) and probed with a phospho-Akt (Ser-473) antibody (1:1000; Cell Signaling, Danvers, MA) followed by a HRP-conjugated goat anti-rabbit antibody (1:10,000; Pierce). The blots were visualized using a SuperSignal West Femto kit (Pierce) and ChemiDoc XRS+ Imaging System (Bio-Rad). Blots were also probed with a monoclonal Actb antibody (1:5000; Sigma) followed by a HRP-conjugated goat anti-mouse antibody (1:20,000; Pierce).

Total RNA Isolation, cDNA Synthesis, and Quantitative PCR—Before myotubes were harvested for total RNA isolation, they were preincubated in the supplement-free DMEM/F-10 (primary myotubes) or DMEM (L6/ZnT7-Myc and L6/vec myotubes) for 3 h and then insulin-treated (0, 10, or 100 nM) at 37 °C for 7 min. Cells were lysed in 1.0 ml TRIzol (Invitrogen). Total RNA was purified according to the manufacturer's protocol. Two μg of total RNA was converted into cDNAs using a high capacity RNA-to-cDNA kit (Applied Biosystems, Foster City, CA). For quantitative RT-PCR analysis, synthesized cDNAs were diluted 5-fold with double-distilled water, and 2 μl was used in a SYBR Green-based PCR (iTaq SYBR Green Supermix with ROX, Bio-Rad). Quantitative PCR was performed on a PRISM ABI 7900HT sequence detection system (Applied Biosystems). All primers were designed by the Primer Express 2.0 software (Applied Biosystems), and the primer

sequences are listed in supplemental Table 1. Melting temperature analysis for the reference genes (*Actb* and *β2m*) and target genes (*Insr* (insulin receptor), *Irs1*, *Irs2*, *Akt1*, and *Glut4* (glucose transporter 4)) revealed a single sharp peak at a typical melting temperature for each examined gene. In addition, PCR amplification efficiency for each reference and target gene was determined. It showed that all genes examined were amplified with similar efficiency (close to 100%; data not shown). cDNA samples were run in triplicate, and the average crossing point value was used for calculations using REST® 2009 software (Qiagen, Valencia, CA). The expression of the target genes was normalized to the expression of the *Actb* and *β2m* reference genes.

Oral Glucose Tolerance Test—Znt7 KO and control mice were fed either a low or high fat diet at 5 weeks of age for 10 weeks. Before the test, mice were fasted for 16–18 h and weighed. Mice were then given 1.5 g of glucose/kg of body weight through a gavage tube. Blood was collected from the tail vein at 0, 30, 60, and 120 min after the glucose load. Blood glucose and serum insulin levels were determined using a One-Touch UltraMini meter (LifeScan) and a mouse ultrasensitive insulin ELISA kit (ALPCO), respectively.

Insulin Tolerance Test—Znt7 KO and control mice were fed a high fat diet at 5 weeks of age for 10 weeks. Before the test, mice were fasted for 4 h and weighed. Mice were given 5.5 units of human insulin/kg of body weight intraperitoneally (Lilly). Blood glucose levels were determined at 0, 30, 60, and 120 min after the insulin injection using a One Touch UltraMini meter (LifeScan).

Statistical Analysis—Data are expressed as means ± S.E. The area under the curve was calculated using the linear trapezoidal rule. Statistical analysis was performed using either Student's *t* test or one-way analysis of variance with post hoc Tukey-Kramer multiple comparison test. $p < 0.05$ was considered significant. For the quantitative RT-PCR assay, statistical analysis was done using simple statistical randomization tests by REST 2009 software.

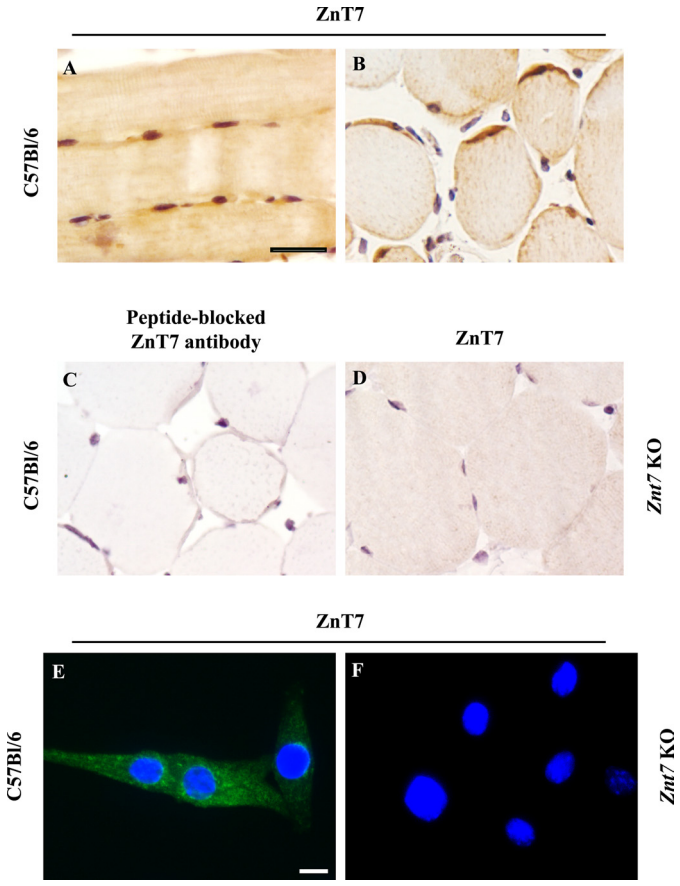

FIGURE 1. **Expression of ZnT7 in mouse skeletal muscles.** Femoral muscles were isolated from male C57Bl/6 and *Znt7* KO mice. Muscles were fixed, embedded, sectioned, and immunostained with either an affinity-purified polyclonal antibody against ZnT7 or a peptide-blocked ZnT7 antibody. *A*, longitudinal section; *B–D*, cross-sections. *A*, *B*, and *D*, muscle fibers were immunostained with the ZnT7 antibody (1:750 dilution); *C*, muscle fibers were immunostained with the peptide-blocked ZnT7 antibody (1:750 dilution). *Black scale bar*, 25 μM. C57Bl/6 (*E*) and *Znt7* KO (*F*) myoblasts were grown in a slide chamber coated with collagen for 48 h before staining. Cells were fixed, permeabilized, and immunostained with the ZnT7 antibody. Immunofluorescent staining of ZnT7 (*green*) was detected in the cytoplasm of myoblasts. The nuclei of myoblasts (*blue*) are indicated by the DAPI staining. *White scale bar*, 10 μM.

RESULTS

ZnT7 Is Expressed in Mouse Skeletal Muscles—In order to examine a potential role of ZnT7 in modulating glucose disposal in skeletal muscles, we first determined the expression of ZnT7 in the mouse skeletal muscle by immunohistochemistry. As shown in Fig. 1, ZnT7 was detected in mouse skeletal muscle fibers. In the longitudinal section of the femoral muscle, ZnT7 was mainly expressed in the sarcoplasm near the nuclei of the fibers (Fig. 1*A*). In the cross-section of the femoral muscle, ZnT7 was detected again in the sarcoplasm near the nuclei at the edges of the fibers (Fig. 1*B*). In the control sections, ZnT7 was not observed in mouse skeletal muscle fibers that were probed with a peptide-blocked ZnT7 antibody (Fig. 1*C*). Skeletal muscle fibers derived from a *Znt7* KO mouse were also probed with the ZnT7 antibody, and no immunostaining of ZnT7 was detected (Fig. 1*D*). In myoblasts isolated from the hind limb skeletal muscle of C57Bl/6 newborn mice, ZnT7 was detected in the cytoplasm of myoblasts with a punctate/tubular pattern (Fig. 1*E*). This immunoreactivity of ZnT7 was not observed in myoblasts isolated from the hind limb skeletal muscle of the *Znt7* KO neonates (Fig. 1*F*).

Insulin-stimulated Phosphorylation of Akt Is Down-regulated in Znt7 KO Primary Myoblasts—We sought to obtain pure populations of skeletal myoblasts from *Znt7* KO and control mice to examine the activity of the insulin signaling pathway in these purified primary myoblasts. The purity of myoblasts was determined by the positive staining of desmin, a muscle-specific intermediate filament protein that is only expressed in myogenic cells (31). The immunostaining assay indicated that the primary cultures (both genotypes) were nearly all myogenic (supplemental Fig. 1). The morphology of myoblasts and the staining pattern of demsin in the myoblasts from *Znt7* KO and control mice were indistinguishable (supplemental Fig. 1).

A decrease in the activity of the insulin signaling pathway is a signature of insulin resistance. We therefore first examined the effect of the *Znt7*-null mutation on the phosphorylation of Akt, a key step in modulating downstream of the insulin signaling pathway (32), in *Znt7* KO and control primary myoblasts. It is

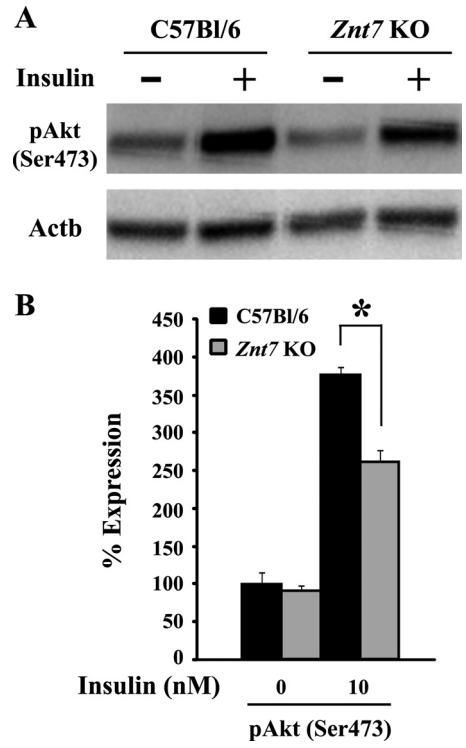

FIGURE 2. **Expression of phosphorylated Akt in primary myoblasts isolated from *Znt7* KO and control mice.** *A*, expression of pAkt. Myoblasts of both genotypes were grown in collagen-coated 6-well plates for 48 h. After incubation of cells in supplement-free medium for 3 h, cells were stimulated by 100 nM insulin at 37 °C for 7 min. Cells were then harvested for Western blot analysis. *A*, representative Western blot is displayed. *B*, densitometry analysis of the Western blot protein bands. The densities of the protein bands of pAkt and Actb were determined by Image Lab 2.0.1 software (Bio-Rad). The expression of pAkt was then normalized by the expression of Actb. Percentage of expression was calculated as the ratio of the normalized value of each sample to that of the corresponding mock-treated control myoblast sample. Three independent primary myoblast preparations from either *Znt7* KO or control skeletal muscles were used in the experiments. Data are reported as mean ± S.E. (*error bars*) of two independent experiments ($n = 6–8$). *, $p < 0.05$.

known that an increased level of phosphorylated Akt after insulin stimulation indicates a high activity of Glut4 exocytosis for glucose uptake (32). Our Western blot results showed that after insulin stimulation, the amount of phosphorylated Akt (pAkt) in *Znt7* KO myoblasts was 30% lower than the control (Fig. 2, *A* and *B*). No difference in the pAkt levels between *Znt7* KO and control myoblasts was observed in the mock-treated myoblasts (Fig. 2*B*).

mRNA Expression of Insulin-responsive Genes Is Down-regulated in Znt7 KO Myotubes—We previously reported that ZnT7 influenced insulin gene expression in pancreatic β-cells (21). Similar regulation might apply to the genes associated with the insulin signaling pathway. To identify potentially differential expression of genes, including *Insr*, *Irs1*, *Irs2*, *Akt1*, and *Glut4*, between *Znt7* KO and control skeletal myotubes, we performed quantitative RT-PCR assays. As shown in Fig. 3*A*, mRNA expression of *Insr* and *Akt1* was decreased by 58% ($p < 0.01$) and 35% ($p < 0.01$), respectively, in *Znt7* KO primary skeletal myotubes compared with the controls. Reduced mRNA expression of *Irs2* (30%) and *Glut4* (25%) in *Znt7* KO myotubes was also observed, although the difference did not reach statistical significance. We also examined the effect of the *Znt7*-null mutation on mRNA expression of these genes in myotubes stimulated with insulin after preincubation of the cells with supplement-free medium for 3 h. As shown in Fig. 3*B*, *Insr* and *Akt1* mRNA expression was down-regulated by 50–60% and 35–60%, respectively, in both mock- and insulin-treated *Znt7* KO myotubes compared with the controls. The reductions of *Insr* and *Akt1* expression were similar to that observed in *Znt7* KO myotubes that were not incubated with supplement-free medium before harvest (Fig. 3*A*), indicating that preincubation of myotubes in supplement-free medium for 3 h did not affect mRNA expression of *Insr* and *Akt1*. The level of *Irs2* mRNA expression was 25% decreased in mock-treated *Znt7* KO myotubes compared with the control ($p < 0.05$), but not in insulin-treated *Znt7* KO myotubes. Finally, insulin treatments appeared to have no effect on the mRNA abundance of *Irs1*, *Irs2*, and *Glut4* in myotubes of both genotypes, except for *Akt1* and *Insr* in *Znt7* KO myotubes. Taken together, these results suggest that the *Znt7*-null mutation results in significant down-regulation of *Insr*, *Akt1*, and *Irs2* mRNA expression in myotubes.

Overexpression of ZnT7 Increases Expression of Irs2 mRNA and Phosphorylation of Irs2 and Akt in Skeletal Myotubes—To further support the results observed in *Znt7* KO primary myotubes, we took an opposite approach to overexpress ZnT7 in skeletal myotubes and then assessed mRNA expression of *Insr*, *Akt1*, *Irs1*, *Irs2*, and *Glut4* and phosphorylation levels of Irs2 and Akt. As shown in Fig. 4*A*, endogenous ZnT7 was readily detected in the cytoplasm as a punctate staining pattern in L6 myoblasts. A similar staining pattern was observed with the exogenous ZnT7 protein in L6 myoblasts stably expressing ZnT7-Myc protein. No significant fluorescent signal was detected in the control cells transfected with the vector. Changes of mRNA expression of *Insr*, *Akt1*, *Irs1*, *Irs2*, and *Glut4* in ZnT7-Myc-expressing L6 myotubes with or without insulin stimulation were examined and compared with the control by quantitative RT-PCR. As demonstrated in Fig. 4*B*, there was a 2-fold increase in *Irs2* mRNA expression in the ZnT7-Myc-expressing L6 myotubes compared with the control in the basal state. Insulin treatment (10 or 100 nM for 7 min) did not affect the abundance of *Irs2* mRNA in ZnT7-Myc-expressing or control L6 myotubes. Furthermore, overexpression of ZnT7 in L6 myotubes did not appear to alter the mRNA expression of *Insr*, *Akt1*, *Irs1*, and *Glut4*.

Overexpression of ZnT7 in L6 myotubes resulted in a significant increase (2-fold, $p < 0.05$) in basal and insulin-stimulated (10 nM for 7 min) phosphorylation of Irs2 (Fig. 4*C*). As expected, the phosphorylation of downstream mediator Akt was also elevated in ZnT7-Myc-expressing L6 myotubes compared with the control after insulin stimulation (10 nM for 7 min, $p < 0.05$) (Fig. 4*D*). These results suggest that ZnT7 has a positive impact on insulin signaling.

Overexpression of ZnT7 in L6 Myotubes Increases Glucose Uptake—Insulin causes Glut4 translocation from an intracellular storage pool to the cell surface of myotubes, leading to an increase in glucose uptake (32). Because ZnT7 had a positive impact on insulin signaling in myocytes (Figs. 2–4), we next examined whether overexpression of ZnT7 in myotubes had a direct effect on glucose uptake. L6/ZnT7-Myc-expressing and control myotubes were stimulated with 0, 10, or 100 nM insulin

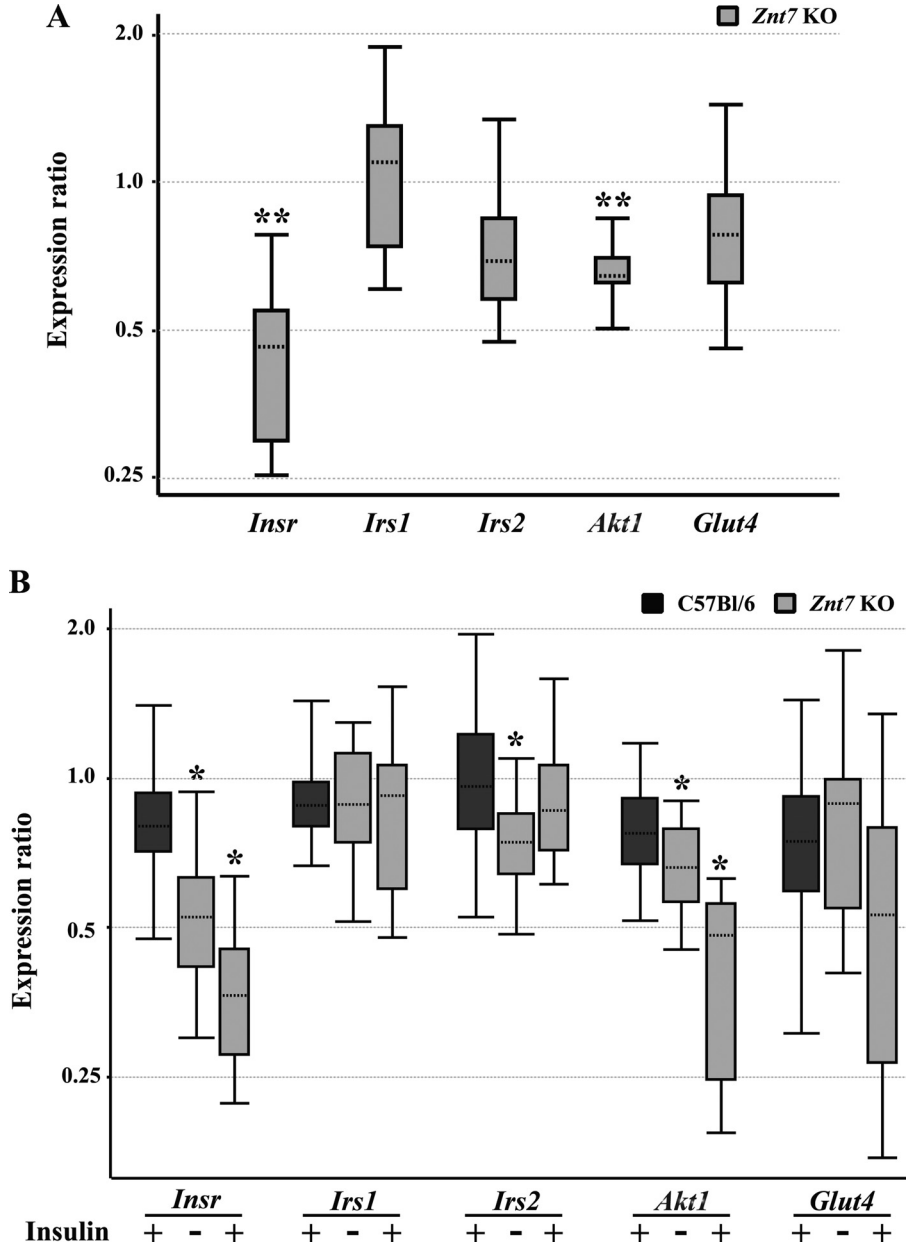

FIGURE 3. **mRNA expression of insulin-responsive genes in *Znt7* KO and control myotubes.** Myoblasts of both genotypes were allowed to differentiate for 6 days before harvest for total RNA isolation or for insulin treatment before RNA isolation. The amount of the target mRNA was measured by a SYBR-based quantitative RT-PCR and analyzed using REST 2009 software (45). *Actb* and *β2m* were used as the internal references, and two independent experiments, each with three independent primary myotube lines (both genotypes), were performed. Data were plotted as *whisker boxes* representing the relative transcription levels of *Insr*, *Irs1*, *Irs2*, *Akt1*, and *Glut4*. The *horizontal dotted lines* in the *boxes* represent the median values, and the *boxes* represent the middle 50% of the observations. The *top* and *bottom whiskers* (*vertical lines*) represent the upper 25% and lower 25% of observations, respectively. *A*, myotubes of both genotypes were harvested for total RNA isolation and quantitative RT-PCR analysis after a 6-day differentiation. The expression of *Insr*, *Irs1*, *Irs2*, *Akt1*, and *Glut4* in *Znt7* KO myotubes was compared with their transcription in the wild type control. **, $p < 0.01$. *B*, after differentiation, myotubes of both genotypes were preincubated with supplement-free medium for 3 h followed by either 0 or 100 nM insulin treatment (7 min) before harvest. The expression of *Insr*, *Irs1*, *Irs2*, *Akt1*, and *Glut4* in the indicated samples was compared with their transcription in the 0 nM insulin-treated controls. *, $p < 0.05$.

for 15 min, followed by 10 μM [^{14}C]2-DG uptake in the presence of 100 μM cold glucose for 15 min. The results showed that, in the control myotubes, insulin at 10 and 100 nM concentrations stimulated 2-DG uptake by 10% ($p < 0.05$) and 27% ($p < 0.01$), respectively. However, in the myotubes expressing ZnT7-Myc, the 2-DG uptake increased to 23% ($p < 0.05$) and 42% ($p < 0.01$), respectively (Fig. 5). On the other hand, the basal 2-DG uptake in both ZnT7-Myc-expressing and control myotubes was similar (Fig. 5). Taken together, these results indicated that in the presence of insulin overexpression of ZnT7 in myotubes increased glucose uptake by 1.5–2-fold.

High Fat Diet Induces Obesity in Znt7 KO and Control Mice—The influence of ZnT7 on the insulin signaling pathway and glucose uptake in skeletal myocytes prompted us to examine the glucose metabolic status of *Znt7* KO mice that were challenged with a high fat diet. We hypothesized that *Znt7* KO mice fed a high fat diet would be more susceptible to diet-induced diabetes than the control due to decreased activity of

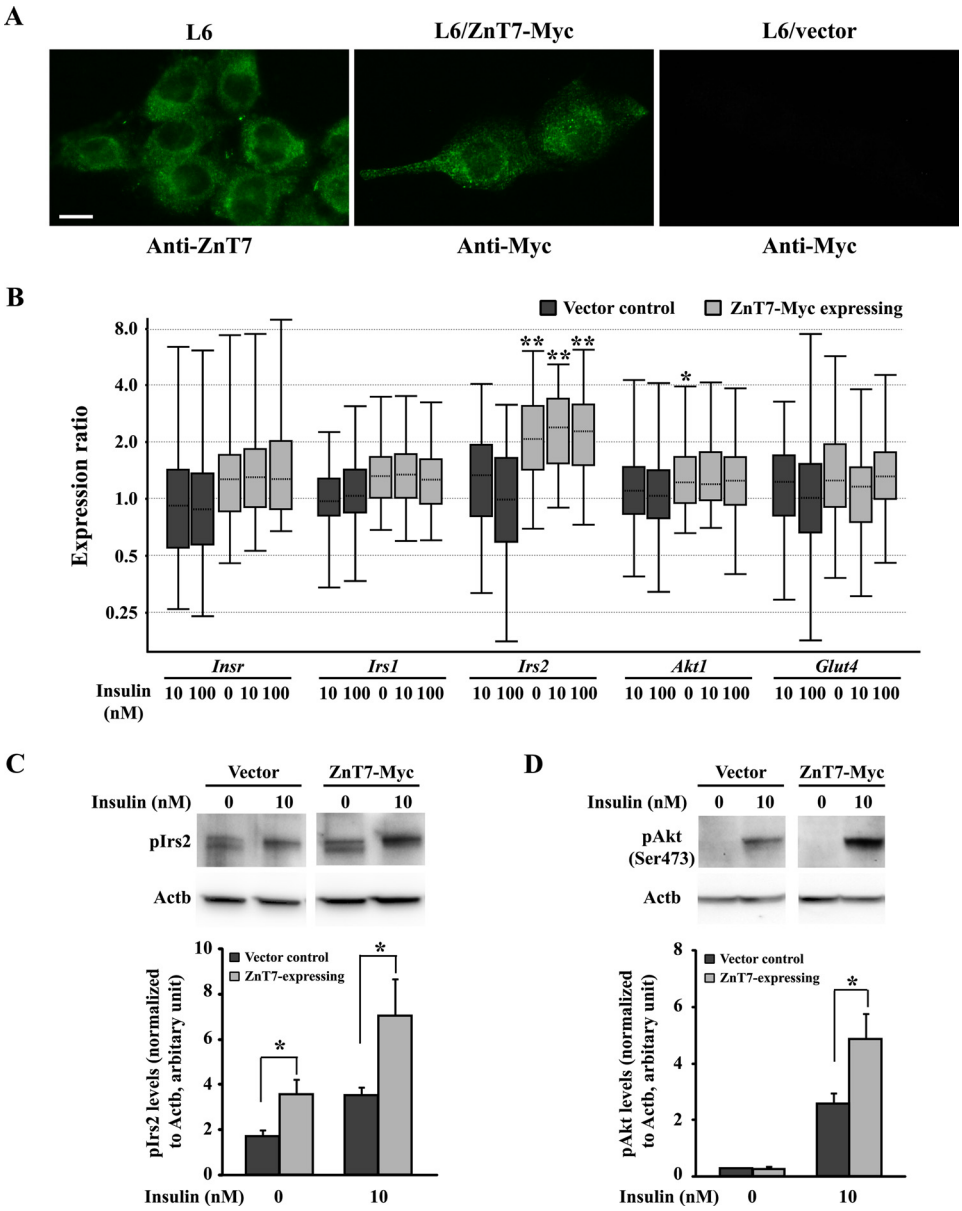

FIGURE 4. **Analysis of L6 cells expressing ZnT7-Myc protein.** *A*, subcellular localization of endogenous ZnT7 or exogenous ZnT7-Myc protein in L6 myoblasts. Cells were grown in the complete α-MEM for 48 h before staining. ZnT7 was detected by the ZnT7 antibody (20), and ZnT7-Myc was detected by the Myc antibody. *B*, mRNA expression of insulin-responsive genes in ZnT7-Myc-expressing or vector control L6 myotubes. ZnT7-Myc-expressing and vector control L6 myoblasts were allowed to differentiate for 6 days to myotubes. Myotubes were then preincubated in supplement-free DMEM at 37 °C for 3 h and treated with 0, 10, or 100 nM insulin at 37 °C for 7 min before harvest. The amount of the target mRNA was measured by a SYBR-based quantitative RT-PCR and analyzed using REST 2009 software (45). *Actb* and *β2m* were used as the internal references. The data were obtained from three individual L6 stable cell lines for either ZnT7-Myc-expression or vector control. The experiments were performed twice in duplicate. The data were plotted as *whisker boxes* representing the relative transcription levels of *Insr*, *Irs1*, *Irs2*, *Akt1*, and *Glut4*. The *horizontal dotted lines* in the *boxes* represent the median values, and the *boxes* represent the middle 50% of the observations. The *top* and *bottom whiskers* (*vertical lines*) represent the upper 25% and lower 25% of observations, respectively. The expression of *Insr*, *Irs1*, *Irs2*, *Akt1*, and *Glut4* in the indicated samples was compared with the expression of the genes in 0 nM insulin-treated L6 vector control cells. *C*, expression of phosphorylated Irs2. *D*, expression of phosphorylated Akt. ZnT7-Myc-expressing myotubes and vector control were preincubated with supplement-free medium for 3 h followed by either 0 or 10 nM insulin treatment (7 min) before harvest. The densities of the protein bands of pIrs2, pAkt, and Actb were determined by Image Lab 2.0.1 software (Bio-Rad). The expression of pIrs2 and pAkt was normalized to the expression of Actb. Three individual L6/ZnT7-Myc and three individual control myotube lines were used in the experiments. Data are reported as mean ± S.E. (*error bars*) of three independent experiments ($n = 9–10$). *, $p < 0.05$; **, $p < 0.01$.

the insulin signaling pathway caused by ZnT7 deficiency (Figs. 2 and 3). To investigate our hypothesis, we fed *Znt7* KO and control mice (C57Bl/6) a high fat diet (45% kcal, HF) starting at 5 weeks of age for 12 weeks. For the dietary fat control, we also fed 5-week-old *Znt7* KO and control mice a low fat diet (10% kcal, LF) for 12 weeks. As shown in Fig. 6*A*, male *Znt7* KO and control mice fed the HF diet gained significantly more weight than the mice of the same genotype fed the LF diet during the feeding period ($p < 0.01$, one-way analysis of variance). Female mice of both genotypes fed the HF diet also gained more weight than the same genotype mice in the LF diet group, but it was not statistically significant ($p > 0.05$, one-way analysis of variance) (Fig. 6*B*). Both male and female *Znt7* KO mice in either the high or low fat diet group weighed less than the control mice in the

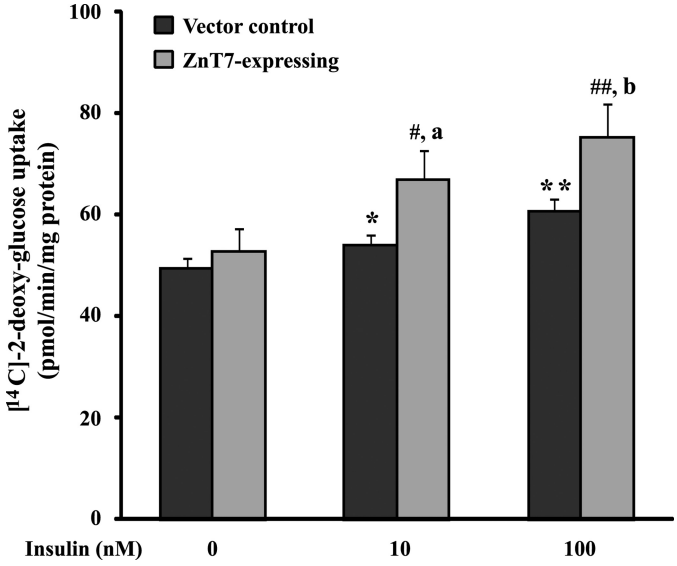

FIGURE 5. **[^{14}C]2-DG uptake in L6/ZnT7-Myc and control myotubes.** L6/ZnT7-Myc and control myoblasts were allowed to differentiate to myotubes and preincubated with medium containing 0.2% FBS for 16 h before the uptake assay. Cells were then serum-starved in α-MEM containing 75 μM $ZnSO_4$ for 4 h, followed by a 60-min incubation in KRH buffer containing 75 μM $ZnSO_4$. Insulin (0, 10, or 100 nM) was added for 15 min, followed by 10 μM [^{14}C]2-DG plus 100 μM unlabeled glucose for 15 min. The [^{14}C]2-DG uptake was expressed per min per mg of lysate protein. Two individual cell lines of L6/ZnT7-Myc and two individual control cell lines were used in the uptake experiments. Data are reported as mean ± S.E. (*error bars*) of three independent experiments in triplicate ($n = 16–18$). *, $p < 0.05$ *versus* control basal; **, $p < 0.01$ *versus* control basal; #, $p < 0.05$ *versus* L6/ZnT7 basal; ##, $p < 0.01$ *versus* L6/ZnT7 basal; *a*, $p < 0.05$ *versus* control treated with 10 nM insulin; *b*, $p < 0.05$ *versus* control treated with 100 nM insulin.

same dietary group during the feeding period ($p < 0.01$, one-way analysis of variance) (Fig. 6, *A* and *B*).

We noticed that although male *Znt7* KO mice weighed less than the control mice during the feeding period in both HF and LF dietary groups, the total body weight gains after 12-week feeding were similar between the two genotypes (Fig. 6*A*, *inset*). On the other hand, female *Znt7* KO mice in both dietary groups gained less body weight than the control mice in the same dietary group during the feeding period (Fig. 6*B*, *inset*, $p < 0.05$).

Znt7 KO Mice Have Less Body Fat on the High Fat Diet—High fat diets lead to increased fat mass in mice. It has been demonstrated that *Znt7* KO mice weigh less than the control due to a decrease in body fat (22). We therefore determined the weight of four major fat pads dissected from mice (epididymal/ovarian, femoral, retroperitoneal, and mesenteric) at the end of the feeding study. After 12 weeks on the HF diet, both *Znt7* KO and control mice had significantly higher fat pad weight than the same genotype mice in the LF dietary group ($p < 0.01$; Fig. 7, *A* and *B*). However, gains in combined fat pad weight of *Znt7* KO of both genders were less than the respective controls ($p < 0.01$). No significant difference in the weight of the four fat pads was observed between *Znt7* KO and controls of both genders in the LF dietary group (Fig. 7, *A* and *B*). Body composition of the remaining carcasses (without the four fat pads mentioned above) showed increased body fat mass expressed in either an absolute term or as a percentage of fat in both genotype mice fed the HF diet ($p < 0.05$; Fig. 7, *C–F*). However, no difference in lean or ash mass was detected between *Znt7* KO and control mice fed the HF diet. In addition, fat, lean, and ash weights did not differ between *Znt7* KO and control mice of both genders in the LF dietary group (Fig. 7, *C–F*).

High Fat Diet Induces Hypercholesterolemia and Hyperglycemia in Mice—To determine the physiological consequences of high fat diet feeding on blood triglyceride, cholesterol, glucose, and insulin levels in *Znt7* KO mice, fasting and non-fasting blood were collected from a cohort of *Znt7* KO and control mice after 12-week exposure to the specific diet (low or high fat diet). Blood glucose, serum triglyceride, cholesterol, and insulin concentrations were determined. As shown in Table 1, the high fat diet induced hypercholesterolemia in both genotypes. The increased fasting serum cholesterol level in *Znt7* KO mice fed the HF diet was similar to that of the control in the same dietary group. Fasting serum triglyceride levels were not significantly changed after 12 weeks of HF diet feeding in male *Znt7* KO and control mice. Notably, the fasting serum triglyceride level in female *Znt7* KO mice was about 50% lower than that in the control mice regardless of dietary treatments ($p < 0.05$).

Blood glucose and serum insulin levels were measured in *Znt7* KO and control mice after a 10-week exposure to the high fat diet to determine whether *Znt7* KO mice were more vulnerable to the diet-induced hyperglycemia and insulin resistance than the control. As shown in Table 2, fasting and non-fasting blood glucose levels were high in both *Znt7* KO and control mice after prolonged exposure to the high fat diet compared with the same genotype mice in the low fat dietary group ($p < 0.05$). Among the mice examined, male *Znt7* KO mice in the high fat dietary group showed a marked increase in the non-fasting glucose level compared with that of the control in the same dietary group ($p < 0.05$). Female *Znt7* KO mice in the high fat dietary group exhibited the same trend, but it was much less apparent. In addition, serum insulin levels were increased along with the increased blood glucose in male *Znt7* KO and control mice fed the high fat diet (Table 3), suggesting insulin resistance. Male *Znt7* KO mice had a low fasting serum insulin level compared with the control in either the low or high fat dietary group, which is consistent with our previous finding that ZnT7 is involved in regulation of insulin synthesis/secretion (21). No significant difference was observed in serum insulin levels in female *Znt7* KO and control mice from both low and high fat dietary groups.

Znt7 KO Mice Fed the High Fat Diet Have More Severe Impairment of Glucose Tolerance—Given that *Znt7* KO mice had low activity of the insulin signaling pathway demonstrated in the isolated myoblasts and myotubes (Figs. 2 and 3) and a higher non-fasting blood glucose level than the control after 10-week feeding of a high fat diet, we next performed oral glucose tolerance tests on *Znt7* KO and control mice to illustrate the physiological importance of ZnT7 action in glucose control. As shown in Fig. 8, *A* and *B*, both *Znt7* KO and control mice (male) displayed impaired glucose tolerance after 10 weeks of high fat diet exposure. However, male *Znt7* KO mice had more pronounced hyperglycemia than the control during the oral glucose tolerance test ($p < 0.05$). Interestingly, male *Znt7* KO mice fed the LF diet also displayed glucose intolerance compared with the control ($p < 0.05$). The glucose intolerance of male *Znt7* KO mice was also illustrated with the area under the

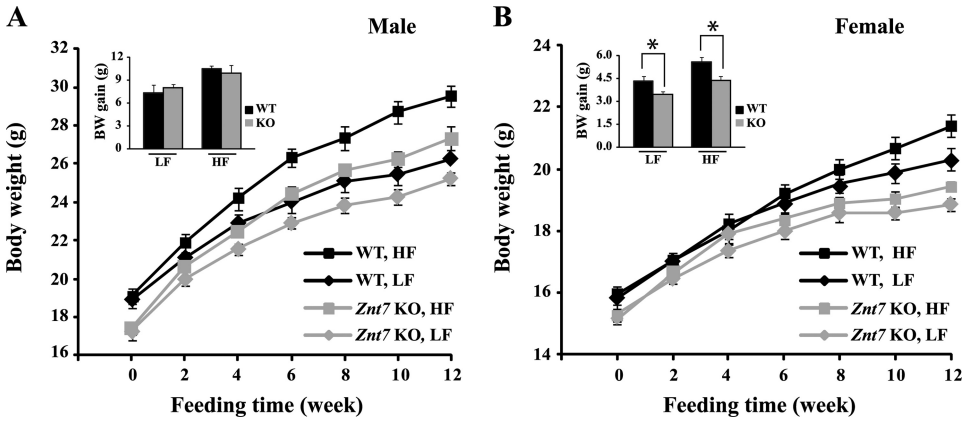

FIGURE 6. **Growth curves and body weight gains of *Znt7* KO and control mice fed either the low or high fat diet.** *A*, male; *B*, female. Mice were fed either a low or a high fat diet at 5 weeks of age for 12 weeks, and body weights were measured at the indicated time points after mice were fed the special diet. All values are expressed as mean ± S.E. (*error bars*), $n = 9–13$/group. The *insets* are summaries of the total body weight gains of male and female *Znt7* KO and control mice after 12-week feeding of the indicated diet. Values are mean ± S.E., $n = 9–13$/group. *, $p < 0.05$. *BW*, body weight; *WT*, C57Bl/6 mice; *KO*, *Znt7* knock-out mice.

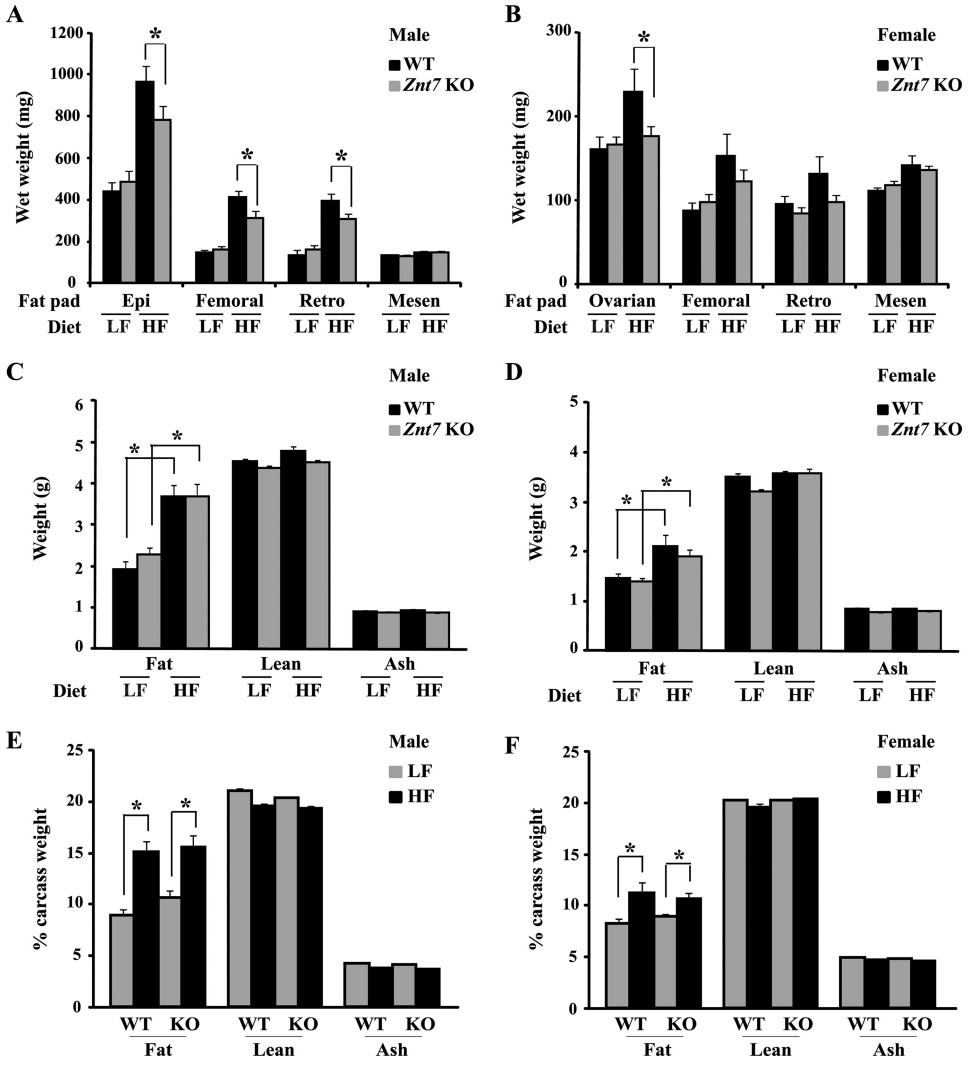

FIGURE 7. **Fat pad weights and body compositions of *Znt7* KO and control mice.** Mice were fed either the low or high fat diet at 5 weeks of age for 12 weeks. Mice were fasted for 16–18 h. Fat pad weights of male (*A*) and female (*B*) are displayed as wet weights (mg). Body compositions are expressed as weight (g) for male (*C*) and female (*D*) and as percentage for male (*E*) and female (*F*). Values are mean ± S.E. (*error bars*), $n = 9–13$/group. *, $p < 0.05$. *WT*, C57Bl/6 mice; *Epi*, epididymal fat; *Retro*, retroperitoneal fat; *Mesen*, mesenteric fat.

TABLE 1

Fasting serum triglyceride and cholesterol levels in *Znt7* KO and control mice

Values are mean ± S.E. Serum was collected from 16–18-h fasted *Znt7* KO and control mice after 12-week feeding.

Genotype	Diet	Male			Female		
		n	Triglycerides	Cholesterol	*n*	Triglycerides	Cholesterol
			mg/ml	*mg/dl*		*mg/ml*	*mg/dl*
C57Bl/6	LF	12	31.3 ± 3.8	97.3 ± 5.9	7	24.5 ± 4.7	75.6 ± 3.8
Znt7 KO	LF	8	36.1 ± 5.6	98.2 ± 2.1	14	11.7 ± 1.2[a]	66.2 ± 2.5
C57Bl/6	HF	11	44.2 ± 7.7	120.7 ± 3.3[b]	13	23.1 ± 4.0	87.2 ± 3.1[b]
Znt7 KO	HF	7	42.6 ± 4.8	123.1 ± 3.1[b]	14	12.5 ± 1.5[a]	80.3 ± 3.3[b]

[a] $p < 0.05$ *versus* control mice in the same dietary group.
[b] $p < 0.05$ *versus* the same genotype mice fed the LF diet.

TABLE 2

Fasting and non-fasting blood glucose levels in *Znt7* KO and control mice

Values are mean (mg/dl) ± S.E. *n* is shown in parentheses. Non-fasting blood glucose was measured between 0830 and 0900 h from non-fasted *Znt7* KO and control mice after 10-week feeding. Fasting blood glucose was measured after 16–18-h fasting.

Genotype	Diet	Male		Female	
		Fasting	Non-fasting	Fasting	Non-fasting
		mg/dl		*mg/dl*	
C57Bl/6	LF	92.9 ± 3.3 (19)	165.5 ± 10.7 (8)	80.8 ± 6.7 (8)	144.6 ± 8.0 (7)
Znt7 KO	LF	80.6 ± 3.5 (12)	181 ± 8.8 (5)	79.1 ± 5.1 (14)	162.8 ± 3.8 (6)
C57Bl/6	HF	115.1 ± 6.2[a] (19)	194.1 ± 10.6 (12)	108.3 ± 3.1[a] (14)	167.0 ± 6.3[a] (8)
Znt7 KO	HF	98.8 ± 6.0[a] (13)	280.6 ± 23.0[a,b] (9)	91.8 ± 5.4 (13)	183.2 ± 8.6 (10)

[a] $p < 0.05$ *versus* the same genotype mice fed the LF diet.
[b] $p < 0.05$ *versus* the control mice in the same dietary group.

TABLE 3

Fasting and non-fasting serum insulin levels in *Znt7* KO and control mice

Values are mean (ng/ml) ± S.E. *n* is shown in parentheses. Non-fasting serum was collected between 0830 and 0900 h from non-fasted *Znt7* KO and control mice after 10-week feeding. Fasting serum was collected from 16–18-h fasted *Znt7* KO and control mice after 10–12-week feeding.

Genotype	Diet	Male		Female	
		Fasting	Non-fasting	Fasting	Non-fasting
		ng/ml		*ng/ml*	
C57Bl/6	LF	0.21 ± 0.04 (19)	0.83 ± 0.20 (6)	0.22 ± 0.03 (8)	0.61 ± 0.04 (7)
Znt7 KO	LF	0.11 ± 0.01[a] (12)	0.78 ± 0.21 (5)	0.18 ± 0.03 (14)	0.76 ± 0.17 (5)
C57Bl/6	HF	0.33 ± 0.04[b] (19)	1.95 ± 0.29[b] (5)	0.18 ± 0.01 (14)	0.43 ± 0.04 (8)
Znt7 KO	HF	0.20 ± 0.03[a,b] (13)	1.77 ± 0.34[b] (6)	0.17 ± 0.02 (14)	0.70 ± 0.12 (10)

[a] $p < 0.05$ *versus* control mice in the same dietary group.
[b] $p < 0.05$ *versus* the same genotype mice fed the LF diet.

curve (AUC) measurement (Fig. 8*C*). The AUC measurement also showed that female *Znt7* KO mice fed the HF diet had slightly impaired glucose clearance compared with the female KO mice fed the LF diet (Fig. 8*C*). Serum insulin levels in male *Znt7* KO mice during the 2-h time course of the assay were lower than that in the controls in both dietary groups (Fig. 8*D*). This was also reflected in the AUC data for insulin (Fig. 8*E*), suggesting a low insulin production after the glucose load in male *Znt7* KO mice (Fig. 8, *D* and *E*). Nevertheless, there was no significant difference in oral glucose tolerance between female *Znt7* KO and control mice in either dietary group.

Because male *Znt7* KO mice had low serum insulin levels during the oral glucose tests, we next performed intraperitoneal insulin tolerance tests on *Znt7* KO and control mice fed the high fat diet to find out whether insulin resistance would also be a factor that contributed to the pronounced glucose intolerance in *Znt7* KO mice. As shown in Fig. 9*A*, intraperitoneal insulin tolerance tests demonstrated that male *Znt7* KO mice fed the HF diet were more resistant to the blood glucose-lowering effect of exogenously administered insulin. This was also reflected by the $AUC_{glucose}$ measurements (Fig. 9*C*). In contrast, similar insulin sensitivities were observed between female *Znt7* KO and control mice fed the high fat diet (Fig. 9*B*). Taken together, these data suggest that impaired glucose clearance in male *Znt7* KO mice may result from both low insulin secretion and low insulin sensitivity in the peripheral tissues. Male *Znt7* KO mice were more susceptible to glucose intolerance than female *Znt7* KO mice after high fat diet feeding.

DISCUSSION

Our laboratory previously reported that the null mutation of the *Znt7* gene led to growth retardation in mice (20). However, despite their low body weight gain, *Znt7* KO mice displayed slightly elevated blood glucose levels 2 h after an oral glucose challenge, suggesting that glucose homeostasis might be affected by the null mutation of *Znt7* (22). Additionally, we demonstrated that ZnT7 influenced insulin synthesis and secretion in the pancreatic β-cell (21). Insulin is a major factor in stimulating glucose uptake in peripheral tissues after a glucose load. Therefore, impaired pancreatic β-cell function and insulin secretion lead to a delayed glucose clearance after a meal. On the other hand, defects in the response of insulin stimulation in peripheral tissues, especially the skeletal muscle that accounts for ~80% of the glucose uptake after a meal, result in insulin resistance. Lack of ZnT7 expression in pancreatic β-cells of *Znt7* KO mice may negatively affect insulin synthesis and secretion in the cell, leading to an abnormal glucose homeostasis.

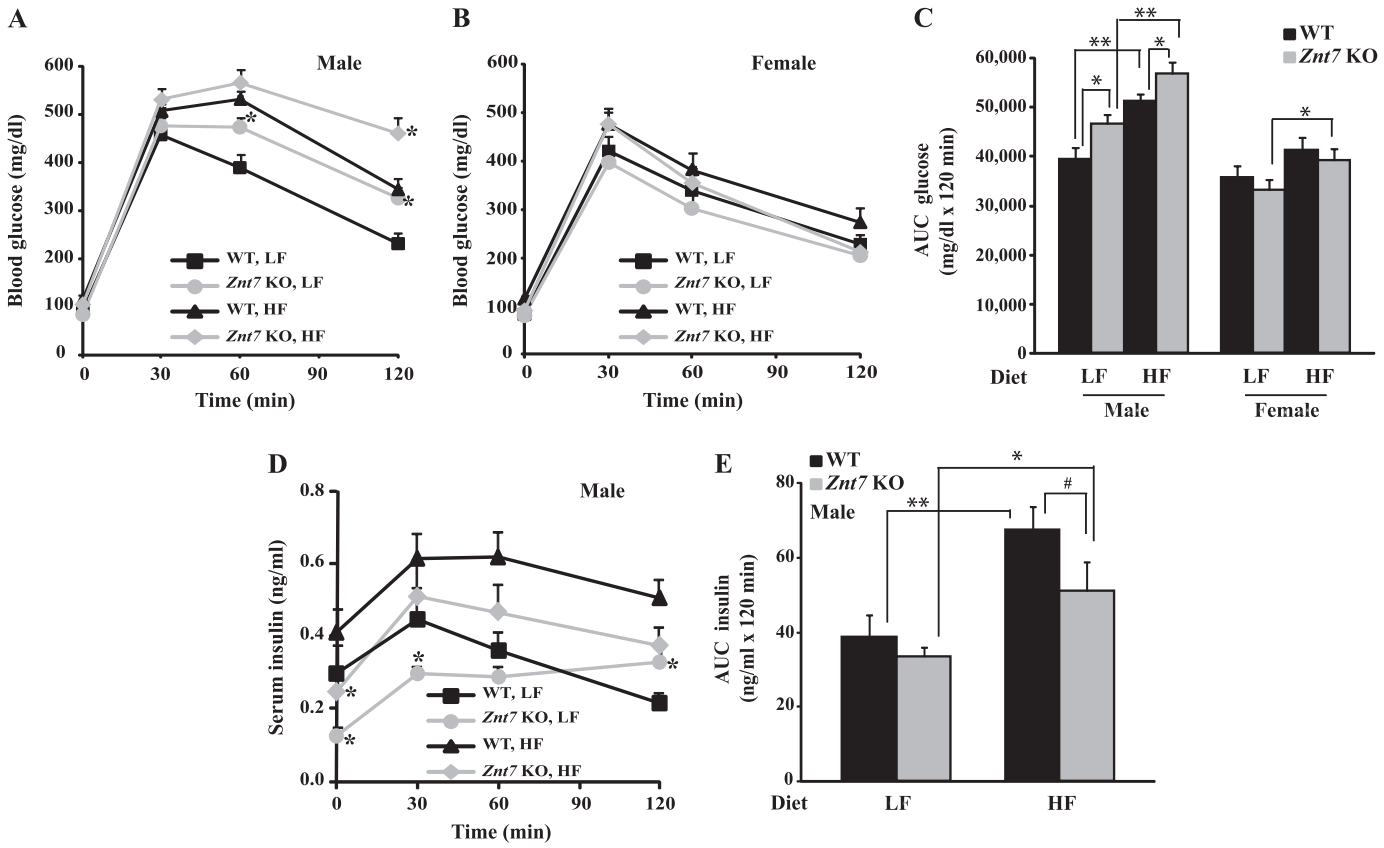

FIGURE 8. **Blood glucose and serum insulin levels in *Znt7* KO and control mice during oral glucose tolerance tests.** Mice were fed either the low or high fat diet at 5 weeks of age for 10 weeks and fasted for 16–18 h before the test. Blood was collected at the indicated time points after the oral glucose load. *A* and *B*, blood glucose levels in male and female mice, respectively, during the oral glucose tolerance test. *C*, area under the curve for glucose (*AUC glucose*). *D*, serum insulin levels in male *Znt7* KO and control mice during the oral glucose tolerance test. Values are the mean ± S.E. (*error bars*), $n = 11–14$/group. *E*, area under the curve for insulin (*AUC insulin*). Values are the mean ± S.E., $n = 7–11$/group. *, $p < 0.05$; **, $p < 0.01$; #, $p = 0.05$.

In the present study, we investigated the effects of the *Znt7*-null mutation on glucose homeostasis, diet-induced hyperglycemia, and insulin resistance in mice. We demonstrated that ZnT7 was expressed in the mouse skeletal muscle and localized in the cytoplasm of the myoblast with a punctate/tubular staining pattern. The activity of the insulin signaling pathway in the myocytes deficient for the ZnT7 expression was down-regulated in the basal and insulin-stimulated states at the transcriptional and post-transcriptional levels. These changes may contribute to the severe glucose intolerance and insulin resistance observed in male *Znt7* KO mice fed a high fat diet. Male and female *Znt7* KO mice responded differently to the diet-induced obesity. Male *Znt7* KO mice responded in the same way as the control mice after introduction of a high fat diet in terms of body weight gain. In contrast, female *Znt7* KO mice were partially resistant to the diet-induced body weight gain. Both male and female *Znt7* KO mice had lower body weights than the controls in both low and high fat dietary groups throughout the feeding period, which may be due to mild zinc deficiency of *Znt7* KO mice. In addition, diet-induced weight gain and subsequent metabolic symptoms were not apparent in female mice of both genotypes in this study. This result is probably due to the fact that female mice require a higher fat diet to develop diabetes (33).

The postprandial hyperglycemia, severe glucose intolerance, decreased circulating insulin, and reduced insulin-sensitivity in male *Znt7* KO mice after 10 weeks on the high fat diet provide *in vivo* evidence for a direct role of ZnT7 in the regulation of glucose homeostasis. Decreased fasting blood insulin observed in male *Znt7* KO mice, regardless of dietary treatments, supports our previous finding that ZnT7 positively influences insulin expression and secretion (21). An unexpected finding of this study was the down-regulation of *Irs2* mRNA expression in the isolated *Znt7* KO myocytes, whereas its expression and phosphorylation were up-regulated in ZnT7-Myc-expressing L6 myotubes. The insulin receptor substrate (Irs) proteins play a critical role in signal transduction from the insulin receptor, a tyrosine kinase that is able to autophosphorylate upon insulin binding. Phosphorylated Irs proteins bind to SH2 domain-containing signaling molecules to trigger phosphorylation of Akt, which in turn stimulates translocation of Glut4 from the interior of the cell to the surface for glucose uptake (34). Consistent with the enhanced insulin signaling in ZnT7-Myc-expressing L6 myotubes, the glucose uptake in these cells also enhanced significantly, suggesting that perturbed zinc metabolism in skeletal muscles can lead to insulin resistance.

Four mammalian Irs proteins have been identified with different tissue distribution (35–38). Irs1 and Irs2, both ubiquitously expressed proteins, have been studied most extensively. The *Irs1*-null mutation in mice results in growth retardation and mild insulin resistance (39). The lack of severe phenotypes of glucose homeostasis in *Irs1* KO mice can be explained by the

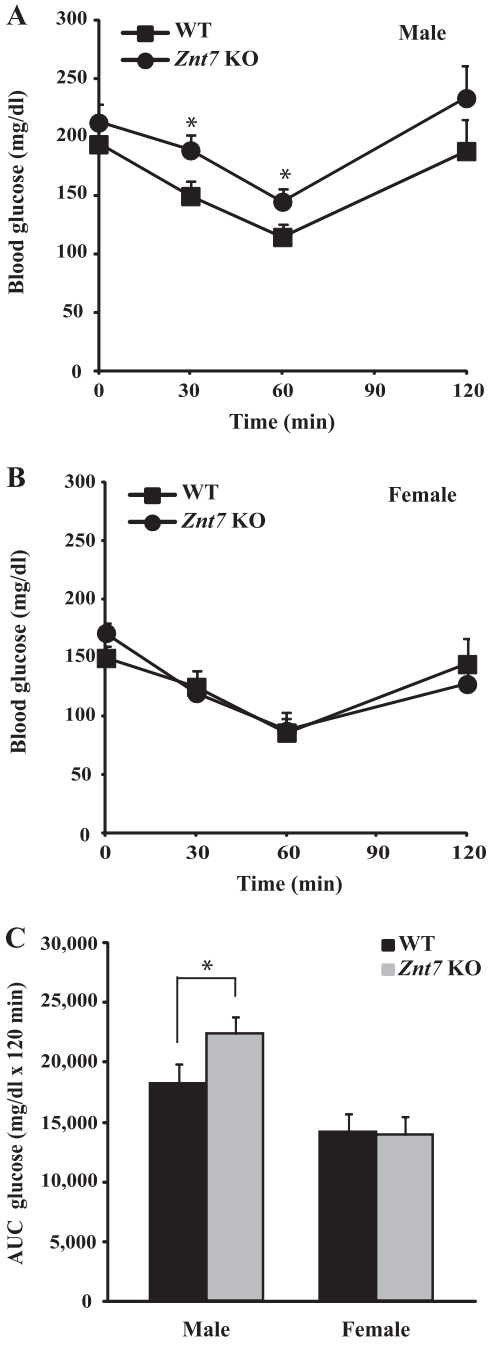

FIGURE 9. **Blood glucose levels in *Znt7* KO and control mice during insulin tolerance tests.** Mice were fed the high fat diet at 5 weeks of age for 10 weeks and fasted for 4 h before the test. Blood was collected at the indicated time points after insulin injection. *A*, male; *B*, female. *C*, area under the curve for glucose (*AUC glucose*). Values are the mean ± S.E. (*error bars*), $n = 8–11$/group. *, $p < 0.05$.

compensation of Irs2 in liver and skeletal muscles of *Irs1* KO mice. On the other hand, *Irs2* KO mice developed diabetes (40). It is thought that inadequate β-cell proliferation, insulin signaling defects in liver, and obesity contribute the diabetic phenotype in *Irs2* KO mice (41, 42). Whether Irs1 and Irs2 mediate distinct insulin receptor signaling in the adult skeletal muscle is currently unknown. In *Znt7* KO mice, the hepatic insulin resistance was not likely to be the cause for the progression of systemic insulin resistance based on two facts: 1) ZnT7 was not detectable in the hepatocytes by Western blot analysis (20) or by immunohistochemistry,[5] and 2) transcriptions of the insulin signaling pathway-associated genes, *Insr*, *Irs1*, *Irs2*, *Akt1*, and *Glut4*, were not altered in the liver of *Znt7* KO mice with insulin resistance (data not shown). The reciprocal regulation of *Irs2* expression in ZnT7- deficient and -overexpressing myotubes suggests that zinc ions may be involved in the regulation of insulin signaling in the skeletal muscle, at least through regulation of *Irs2* mRNA expression. It is not clear whether the low mRNA expression of *Irs2* in skeletal myotubes of *Znt7* KO mice is due to the down-regulation of the promoter activity of *Irs2* or due to a rapid degradation of *Irs2* mRNA.

Irs1 and Irs2 are often expressed together in tissues and cells and can interact with each other to form a heterodimer. However, they are different from each other in responding to cell signals in some distinctive physiological conditions and cellular contexts (43). In the central nervous system, Irs2 plays a role in brain development, nutrient sensing, and life span regulation (44). It is known that zinc deficiency reduces food intake and causes abnormal eating behavior due to changes in taste and smell sensing. The mechanism of action of zinc deficiency on food intake and neurological disorders is currently not understood. *Znt7* KO mice may provide a good model to investigate the possibility of the involvement of Irs2 as a signal protein to link zinc to the neurological changes in the brain in the zinc-deficient state because *Znt7* KO mice are mildly zinc-deficient and have slightly reduced food intake (22).

In conclusion, *Znt7* KO mice were more susceptible to high fat diet-induced postprandial hyperglycemia, glucose intolerance, and insulin resistance. A reduction in insulin secretion and a decrease in the activity of the insulin signaling pathway as a result of down-regulation of *Irs2* gene expression and downstream of Akt phosphorylation in the skeletal muscle may underlie the severe metabolic symptoms in male *Znt7* KO mice fed a high fat diet.

Acknowledgments—We thank the research scientists in the Obesity and Metabolism Research Unit, Western Human Nutrition Research Center, for helpful discussions and support. We thank Erik Gertz and Surapun Tepaamorndech at the Western Human Nutrition Center for experimental assistance.

REFERENCES

1. Palmiter, R. D., and Huang, L. (2004) Efflux and compartmentalization of zinc by members of the SLC30 family of solute carriers. *Pflugers Arch.* **447,** 744–751
2. Kambe, T., Narita, H., Yamaguchi-Iwai, Y., Hirose, J., Amano, T., Sugiura, N., Sasaki, R., Mori, K., Iwanaga, T., and Nagao, M. (2002) Cloning and characterization of a novel mammalian zinc transporter, zinc transporter 5, abundantly expressed in pancreatic beta cells. *J. Biol. Chem.* **277,** 19049–19055
3. Jackson, K. A., Helston, R. M., McKay, J. A., O'Neill, E. D., Mathers, J. C., and Ford, D. (2007) Splice variants of the human zinc transporter ZnT5 (SLC30A5) are differentially localized and regulated by zinc through transcription and mRNA stability. *J. Biol. Chem.* **282,** 10423–10431
4. Eide, D.J. (2004) The SLC39 family of metal ion transporters. *Pflugers*

[5] L. Huang, C. P. Kirschke, Y.-A. E. Lay, L. B. Levy, D. E. Lamirande, and P. H. Zhang, unpublished data.

Arch. **447,** 796–800
5. Valentine, R. A., Jackson, K. A., Christie, G. R., Mathers, J. C., Taylor, P. M., and Ford, D. (2007) ZnT5 variant B is a bidirectional zinc transporter and mediates zinc uptake in human intestinal Caco-2 cells. *J. Biol. Chem.* **282,** 14389–14393
6. Wang, F., Dufner-Beattie, J., Kim, B. E., Petris, M. J., Andrews, G., and Eide, D. J. (2004) Zinc-stimulated endocytosis controls activity of the mouse ZIP1 and ZIP3 zinc uptake transporters. *J. Biol. Chem.* **279,** 24631–24639
7. Staiger, H., Machicao, F., Stefan, N., Tschritter, O., Thamer, C., Kantartzis, K., Schäfer, S. A., Kirchhoff, K., Fritsche, A., and Häring, H. U. (2007) Polymorphisms within novel risk loci for type 2 diabetes determine beta-cell function. *PLoS ONE* **2,** e832
8. Gohlke, H., Ferrari, U., Koczwara, K., Bonifacio, E., Illig, T., and Ziegler, A. G. (2008) SLC30A8 (ZnT8) Polymorphism is associated with young age at type 1 diabetes onset. *Rev. Diabet. Stud.* **5,** 25–27
9. Chimienti, F., Devergnas, S., Pattou, F., Schuit, F., Garcia-Cuenca, R., Vandewalle, B., Kerr-Conte, J., Van Lommel, L., Grunwald, D., Favier, A., and Seve, M. (2006) *In vivo* expression and functional characterization of the zinc transporter ZnT8 in glucose-induced insulin secretion. *J. Cell Sci.* **119,** 4199–4206
10. Chimienti, F., Devergnas, S., Favier, A., and Seve, M. (2004) Identification and cloning of a beta-cell-specific zinc transporter, ZnT-8, localized into insulin secretory granules. *Diabetes* **53,** 2330–2337
11. Boesgaard, T.W., Zilinskaite, J., Vänttinen, M., Laakso, M., Jansson, P. A., Hammarstedt, A., Smith, U., Stefan, N., Fritsche, A., Häring, H., Hribal, M., Sesti, G., Zobel, D. P., Pedersen, O., Hansen, T., and the EUGENE 2 Consortium (2008) The common SLC30A8 R325W variant is associated with reduced first-phase insulin release in 846 non-diabetic offspring of type 2 diabetes patients. The EUGENE2 study. *Diabetologia* **51,** 816–820
12. Wenzlau, J. M., Juhl, K., Yu, L., Moua, O., Sarkar, S. A., Gottlieb, P., Rewers, M., Eisenbarth, G. S., Jensen, J., Davidson, H. W., and Hutton, J. C. (2007) The cation efflux transporter ZnT8 (Slc30A8) is a major autoantigen in human type 1 diabetes. *Proc. Natl. Acad. Sci. U.S.A.* **104,** 17040–17045
13. Wenzlau, J. M., Liu, Y., Yu, L., Moua, O., Fowler, K. T., Rangasamy, S., Walters, J., Eisenbarth, G. S., Davidson, H. W., and Hutton, J. C. (2008) A common nonsynonymous single nucleotide polymorphism in the SLC30A8 gene determines ZnT8 autoantibody specificity in type 1 diabetes. *Diabetes* **57,** 2693–2697
14. Zeggini, E., Weedon, M. N., Lindgren, C. M., Frayling, T. M., Elliott, K. S., Lango, H., Timpson, N. J., Perry, J. R., Rayner, N. W., Freathy, R. M., Barrett, J. C., Shields, B., Morris, A. P., Ellard, S., Groves, C. J., Harries, L. W., Marchini, J. L., Owen, K. R., Knight, B., Cardon, L. R., Walker, M., Hitman, G. A., Morris, A. D., Doney, A. S., the Wellcome Trust Case Control Consortium (WTCCC), McCarthy, M. I., and Hattersley, A. T. (2007) Replication of genome-wide association signals in UK samples reveals risk loci for type 2 diabetes. *Science* **316,** 1336–1341
15. Scott, L. J., Mohlke, K. L., Bonnycastle, L. L., Willer, C. J., Li, Y., Duren, W. L., Erdos, M. R., Stringham, H. M., Chines, P. S., Jackson, A. U., Prokunina-Olsson, L., Ding, C. J., Swift, A. J., Narisu, N., Hu, T., Pruim, R., Xiao, R., Li, X. Y., Conneely, K. N., Riebow, N. L., Sprau, A.G., Tong, M., White, P. P., Hetrick, K. N., Barnhart, M. W., Bark, C. W., Goldstein, J. L., Watkins, L., Xiang, F., Saramies, J., Buchanan, T. A., Watanabe, R. M., Valle, T. T., Kinnunen, L., Abecasis, G. R., Pugh, E. W., Doheny, K. F., Bergman, R. N., Tuomilehto, J., Collins, F. S., and Boehnke, M. (2007) A genome-wide association study of type 2 diabetes in Finns detects multiple susceptibility variants. *Science* **316,** 1341–1345
16. Diabetes Genetics Initiative of Broad Institute of Harvard and MIT, Lund University, and Novartis Institutes of BioMedical Research, Saxena, R., Voight, B. F., Lyssenko, V., Burtt, N. P., de Bakker, P. I., Chen, H., Roix, J. J., Kathiresan, S., Hirschhorn, J. N., Daly, M. J., Hughes, T. E., Groop, L., Altshuler, D., Almgren, P., Florez, J. C., Meyer, J., Ardlie, K., Bengtsson Boström, K., Isomaa, B., Lettre, G., Lindblad, U., Lyon, H. N., Melander, O., Newton-Cheh, C., Nilsson, P., Orho-Melander, M., Råstam, L., Speliotes, E. K., Taskinen, M. R., Tuomi, T., Guiducci, C., Berglund, A., Carlson, J., Gianniny, L., Hackett, R., Hall, L., Holmkvist, J., Laurila, E., Sjögren, M., Sterner, M., Surti, A., Svensson, M., Tewhey, R., Blumenstiel, B., Parkin, M., Defelice, M., Barry, R., Brodeur, W., Camarata, J., Chia, N., Fava, M., Gibbons, J., Handsaker, B., Healy, C., Nguyen, K., Gates, C., Sougnez, C., Gage, D., Nizzari, M., Gabriel, S. B., Chirn, G. W., Ma, Q., Parikh, H., Richardson, D., Ricke, D., and Purcell, S. (2007) Genome-wide association analysis identifies loci for type 2 diabetes and triglyceride levels. *Science* **316,** 1331–1336
17. Pound, L. D., Sarkar, S. A., Benninger, R. K., Wang, Y., Suwanichkul, A., Shadoan, M. K., Printz, R. L., Oeser, J. K., Lee, C. E., Piston, D. W., McGuinness, O. P., Hutton, J. C., Powell, D. R., and O'Brien, R. M. (2009) Deletion of the mouse Slc30a8 gene encoding zinc transporter-8 results in impaired insulin secretion. *Biochem. J.* **421,** 371–376
18. Wijesekara, N., Dai, F. F., Hardy, A. B., Giglou, P. R., Bhattacharjee, A., Koshkin, V., Chimienti, F., Gaisano, H. Y., Rutter, G. A., and Wheeler, M. B. (2010) Beta cell-specific Znt8 deletion in mice causes marked defects in insulin processing, crystallization, and secretion. *Diabetologia* **53,** 1656–1668
19. Lemaire, K., Ravier, M. A., Schraenen, A., Creemers, J. W., Van de Plas, R., Granvik, M., Van Lommel, L., Waelkens, E., Chimienti, F., Rutter, G. A., Gilon, P., in't Veld, P. A., and Schuit, F. C. (2009) Insulin crystallization depends on zinc transporter ZnT8 expression but is not required for normal glucose homeostasis in mice. *Proc. Natl. Acad. Sci. U.S.A.* **106,** 14872–14877
20. Kirschke, C. P., and Huang, L. (2003) ZnT7, a novel mammalian zinc transporter, accumulates zinc in the Golgi apparatus. *J. Biol. Chem.* **278,** 4096–4102
21. Huang, L., Yan, M., and Kirschke, C.P. (2010) Overexpression of ZnT7 increases insulin synthesis and secretion in pancreatic beta-cells by promoting insulin gene transcription. *Exp. Cell Res.* **316,** 2630–2643
22. Huang, L., Yu, Y. Y., Kirschke, C. P., Gertz, E. R., and Lloyd, K. K. (2007) Znt7 (Slc30a7)-deficient mice display reduced body zinc status and body fat accumulation. *J. Biol. Chem.* **282,** 37053–37063
23. Prasad, A. S. (2001) Recognition of zinc deficiency syndrome. *Nutrition* **17,** 67–69
24. Friedman, J. M. (2000) Obesity in the new millennium. *Nature* **404,** 632–634
25. Ahima, R. S., Saper, C. B., Flier, J. S., and Elmquist, J. K. (2000) Leptin regulation of neuroendocrine systems. *Front. Neuroendocrinol.* **21,** 263–307
26. Mantzoros, C. S., Prasad, A. S., Beck, F. W., Grabowski, S., Kaplan, J., Adair, C., and Brewer, G. J. (1998) Zinc may regulate serum leptin concentrations in humans. *J. Am. Coll. Nutr.* **17,** 270–275
27. Shulman, G. I., Rothman, D. L., Jue, T., Stein, P., DeFronzo, R. A., and Shulman, R. G. (1990) Quantitation of muscle glycogen synthesis in normal subjects and subjects with non-insulin-dependent diabetes by ^{13}C nuclear magnetic resonance spectroscopy. *N. Engl. J. Med.* **322,** 223–228
28. Dawson, N. J. (1970) Body composition of inbred mice (*Mus musculus*). *Comp. Biochem. Physiol.* **37,** 589–593
29. Kirschke, C. P., and Huang, L. (2008) Expression of the ZNT (SLC30) family members in the epithelium of the mouse prostate during sexual maturation. *J. Mol. Histol.* **39,** 359–370
30. Richler, C., and Yaffe, D. (1970) The *in vitro* cultivation and differentiation capacities of myogenic cell lines. *Dev. Biol.* **23,** 1–22
31. Kaufman, S. J., and Foster, R. F. (1988) Replicating myoblasts express a muscle-specific phenotype. *Proc. Natl. Acad. Sci. U.S.A.* **85,** 9606–9610
32. Wang, Q., Somwar, R., Bilan, P. J., Liu, Z., Jin, J., Woodgett, J. R., and Klip, A. (1999) Protein kinase B/Akt participates in GLUT4 translocation by insulin in L6 myoblasts. *Mol. Cell. Biol.* **19,** 4008–4018
33. Gajda, A. M., Pellizzon, M. A., Ricci M. R., and Ulman, E. A. (2007) Diet-induced metabolic syndrome in rodent models, in *Animal LAB News*, March 2007
34. Myers, M. G., Jr., Sun, X. J., Cheatham, B., Jachna, B. R., Glasheen, E. M., Backer, J. M., and White, M. F. (1993) IRS-1 is a common element in insulin and insulin-like growth factor-I signaling to the phosphatidylinositol 3′-kinase. *Endocrinology* **132,** 1421–1430
35. Sun, X. J., Wang, L. M., Zhang, Y., Yenush, L., Myers, M. G., Jr., Glasheen, E., Lane, W. S., Pierce, J. H., and White, M. F. (1995) Role of IRS-2 in insulin and cytokine signaling. *Nature* **377,** 173–177
36. Lavan, B. E., Lane, W. S., and Lienhard, G. E. (1997) The 60-kDa phosphotyrosine protein in insulin-treated adipocytes is a new member of the insulin receptor substrate family. *J. Biol. Chem.* **272,** 11439–11443

37. Lavan, B. E., Fantin, V. R., Chang, E. T., Lane, W. S., Keller, S. R., and Lienhard, G. E. (1997) A novel 160-kDa phosphotyrosine protein in insulin-treated embryonic kidney cells is a new member of the insulin receptor substrate family. *J. Biol. Chem.* **272,** 21403–21407
38. White, M. F., Maron, R., and Kahn, C. R. (1985) Insulin rapidly stimulates tyrosine phosphorylation of a M_r 185,000 protein in intact cells. *Nature* **318,** 183–186
39. Tamemoto, H., Kadowaki, T., Tobe, K., Yagi, T., Sakura, H., Hayakawa, T., Terauchi, Y., Ueki, K., Kaburagi, Y., and Satoh, S. (1994) Insulin resistance and growth retardation in mice lacking insulin receptor substrate-1. *Nature* **372,** 182–186
40. Withers, D. J., Gutierrez, J. S., Towery, H., Burks, D. J., Ren, J. M., Previs, S., Zhang, Y., Bernal, D., Pons, S., Shulman, G. I., Bonner-Weir, S., and White, M. F. (1998) Disruption of IRS-2 causes type 2 diabetes in mice. *Nature* **391,** 900–904
41. Suzuki, R., Tobe, K., Aoyama, M., Inoue, A., Sakamoto, K., Yamauchi, T., Kamon, J., Kubota, N., Terauchi, Y., Yoshimatsu, H., Matsuhisa, M., Nagasaka, S., Ogata, H., Tokuyama, K., Nagai, R., and Kadowaki, T. (2004) Both insulin signaling defects in the liver and obesity contribute to insulin resistance and cause diabetes in Irs2(−/−) mice. *J. Biol. Chem.* **279,** 25039–25049
42. Withers, D. J., Burks, D. J., Towery, H. H., Altamuro, S. L., Flint, C. L., and White, M. F. (1999) Irs-2 coordinates Igf-1 receptor-mediated beta-cell development and peripheral insulin signaling. *Nat. Genet.* **23,** 32–40
43. Karlsson, H.K., and Zierath, J.R. (2007) Insulin signaling and glucose transport in insulin-resistant human skeletal muscle. *Cell Biochem. Biophys.* **48,** 103–113
44. Taguchi, A., and White, M. F. (2008) Insulin-like signaling, nutrient homeostasis, and life span. *Annu. Rev. Physiol.* **70,** 191–212
45. Pfaffl, M. W., Horgan, G. W., and Dempfle, L. (2002) Relative expression software tool (REST) for group-wise comparison and statistical analysis of relative expression results in real-time PCR. *Nucleic Acids Res.* **30,** e36